RSC Advances

PAPER

View Article Online
View Journal | View Issue

Cite this: *RSC Adv.*, 2019, **9**, 9533

Novel magnetically separable anhydride-functionalized Fe_3O_4@SiO_2@PEI-NTDA nanoparticles as effective adsorbents: synthesis, stability and recyclable adsorption performance for heavy metal ions

Chaoyang Jia,[a] Junhong Zhao,[a] Liling Lei,[a] Xiyang Kang,[a] Ran Lu,[a] Chongtao Chen,[a] Shunling Li,[b] Yale Zhao,[a] Qingxiang Yang*[a] and Zhijun Chen*[a]

In this paper, a novel adsorbent, Fe_3O_4@SiO_2@PEI-NTDA, was first prepared by the immobilization of an amine and anhydride onto magnetic Fe_3O_4@SiO_2 nanoparticles with polyethylenimine (PEI) and 1,4,5,8-naphthalenetetracarboxylic-dianhydride (NTDA) for the removal of heavy metal ions from aqueous solutions. The structure of Fe_3O_4@SiO_2@PEI-NTDA was systematically investigated; the results confirmed that amine and anhydride groups were successfully covalently grafted onto the surface of Fe_3O_4@SiO_2, which showed a homogenous core–shell structure with three layers of about 300 nm diameter (Fe_3O_4 core: 200 nm, *n*SiO_2 layer: 20 nm, and PEI-NTDA layer: 20 nm). The adsorption performance of Fe_3O_4@SiO_2@PEI-NTDA NPs was evaluated for single Pb^{2+} and coexisting Cd^{2+}, Ni^{2+}, Cu^{2+}, and Zn^{2+} ions in an aqueous solution in a batch system. The amine and anhydride groups may have a synergistic effect on Pb^{2+} removal through electrostatic interactions and chelation; Fe_3O_4@SiO_2@PEI-NTDA NPs exhibited preferable removal of Pb^{2+} with maximum adsorption capacity of 285.3 mg g^{-1} for Pb^{2+} at a solution pH of 6.0, adsorbent dosage of 0.5 g L^{-1}, initial Pb^{2+} concentration of 200 mg L^{-1} and contact time of 3 h. The adsorption mechanism conformed well to the Langmuir isotherm model, and the adsorption kinetic data were found to fit the pseudo-second order model. Fe_3O_4@SiO_2@PEI-NTDA NPs could be recovered easily from their dispersion by an external magnetic field and demonstrated good recyclability and reusability for at least 6 cycles with a high adsorption capacity above 204.5 mg g^{-1}. The magnetic adsorbents showed high stability with a weight loss below 0.65% in the acid leaching treatment by 2 M HCl solution for 144 h. This study indicates that Fe_3O_4@SiO_2@PEI-NTDA NPs are new promising adsorbents for the effective removal of Pb^{2+} in wastewater treatment.

Received 16th December 2018
Accepted 15th February 2019

DOI: 10.1039/c8ra10310k

rsc.li/rsc-advances

1. Introduction

The discharge of wastewaters from various industrial activities, releasing many heavy metal contaminants, such as Cd^{2+}, Ni^{2+}, Cu^{2+} and Pb^{2+}, has become one of the major environmental concerns in recent years.[1] Heavy metal contaminants in such effluents are non-biodegradable and accumulate easily in living organisms through the food chain. Most heavy metals are known to be toxic; they may cause great damage to tissues and organs and even lead to dysmorphia and cancer even at low concentrations,[2] posing a serious threat to human health, animals, plants and urban ecosystems. Among these heavy metals, Pb^{2+} is recognized as one of the most toxic elements; it can damage the kidney, liver, central nervous system, and especially the brain.[3] Therefore, it is extremely essential to eliminate lead ions from waste water prior to its disposal. The maximum permissible levels of lead in drinking water have been established, including 0.010 mg L^{-1} by the EU and 0.015 mg L^{-1} by the US EPA, to protect natural water bodies from being contaminated by effluents containing such a heavy metal.[4]

Several methods have been developed to eliminate heavy metal ion contaminants from their wastewaters including reverse osmosis, co-precipitation,[5] ion exchange,[6] coagulation–flocculation,[7] membrane processes,[8] chemical oxidation,[9] biological processes,[10] chemical treatment,[11] and adsorption.[12] However, all these methods have their own limitations, such as time-consuming procedures, requirement for expensive equipment, and/or continuous need of chemical replenishment. Among these technologies mentioned above, adsorption has been considered to be one of the most common methods for the removal of heavy metal ions because of its ease of operation and

[a]School of Chemical Engineering and Material Science, Zhengzhou University of Light Industry, Zhengzhou 450002, PR China. E-mail: chenzj@zzuli.edu.cn
[b]Jiyuan Institutes of Environmental Science, Jiyuan 459000, PR China

high effectiveness. The key subject in adsorption technologies is to develop an efficient adsorbent with a rapid, selective, cost-effective and highly effective adsorption process; this has received intensive research attention. Thus, a variety of materials, such as activated carbons,[13] zeolites,[14] and biomaterials,[15] have been investigated as adsorbents for heavy metal ion removal from wastewater. However, these adsorbents generally need to be separated from the water treatment system after the adsorption process by methods such as centrifugation or filtration. These inconvenient separation procedures prevent their large-scale applications in water treatment.

Hence, magnetic adsorbent materials, especially Fe_3O_4, have attracted wide interest in environmental remediation programs due to their easy and cost-effective separation processes only by using an external magnetic field and also because of their biocompatibility. However, naked Fe_3O_4 NPs, possessing high surface energy, tend to form aggregations quickly; this eliminates their adsorption properties and magnetic efficiency. Additionally, naked Fe_3O_4 is known to be prone to oxidation and is highly susceptible to leaching under acidic conditions. To stabilize and modify magnetic Fe_3O_4 particles and further improve their adsorption properties, composite materials have been fabricated in core–shell structures with polymers, silica-containing organic materials or other materials as a shell, such as Fe_3O_4@MO_x (M = Si, Mn, Ti, and Al)[16–18] and Fe_3O_4@-polymer.[19] One of the most important methods is the introduction of a dense SiO_2 layer on the surface of magnetite Fe_3O_4 particles, which is very stable in acidic conditions and is inert to redox reactions; thus, it can effectively protect the inner magnetite cores from leaching in an acidic medium in practical applications.[20] Additionally, SiO_2 having abundant hydroxyl groups on its surface can be further modified by other functional groups to improve its properties. Recently, various functional groups have been anchored to the surface of Fe_3O_4@SiO_2 composites to improve their adsorption properties, and these examples include EDTA-modified Fe_3O_4@SiO_2,[21] dimercaptosuccinic acid-coated Fe_3O_4@SiO_2,[22] and (3-aminopropyl) trimethoxysilane-modified Fe_3O_4@SiO_2.[23] Polyethylenimine (PEI), a hydrophilic polymer, has also been frequently used to improve the adsorption properties of materials towards metal ions because of the abundant functional amine groups in its structure.[24] PEI has usually been grafted to other matrices such as insoluble polymers,[25] biomass,[26] and cellulose[27] to prevent its dissociation from the surface of the matrices during adsorption operations; it has also been used to construct magnetic hybrid nanomaterials for environmental applications in heavy metal ion removal.[28–30]

In this work, to synthesize a magnetically separable adsorbent with high stability and adsorption capacity, a new type of magnetic silica material with amine and anhydride-functionalized layers was fabricated by covalently grafting a PEI polymer, followed by anhydride functionalization with 1,4,5,8-naphthalenetetracarboxylic-dianhydride (NTDA) onto the surface of Fe_3O_4@SiO_2, as shown in Scheme 1. The PEI-NTDA layer on Fe_3O_4@SiO_2 not only endowed the final magnetic adsorbents with hydrophilicity, reducing nonspecific adsorption during wastewater treatments, but also provided numerous amine and anhydride groups, which may synergistically coordinate or chelate with heavy metal ions. All these characteristics were expected to endow the final adsorbents with high adsorption capacity of heavy metal ions in wastewater treatments. The properties of the as-prepared Fe_3O_4@SiO_2@-PEI-NTDA adsorbent, including its stability in acid, magnetic performance, reusability, adsorption capacity and adsorption mechanism on Pb^{2+}, were systematically evaluated in this work.

2. Experimental

2.1. Chemicals

The chemicals used in this work were all of analytical grade and were used without any purification treatment. Ferric chloride hexahydrate ($FeCl_3 \cdot 6H_2O$, Tianjin Fengchuan Chemical Reagent Science and Technology Co., Ltd., China), anhydrous sodium acetate (NaAc) and ethylene glycol (EG, both from Aladdin Reagent Co. Ltd., Shanghai, China) were used to prepare the magnetic Fe_3O_4 nanoparticles. Tetraethylorthosilicate (TEOS), ethanol, and ammonium hydroxide (25% w/w) were all purchased from Aladdin and used to prepare SiO_2 on the surface of Fe_3O_4. Methane sulfonic acid (10%, Merck Chemical Technology Co., Ltd., Shanghai, China), 3-chloropropyltrimethoxysilane (Hua Kai Resin Co., Ltd.) and branched polyethyleneimine (PEI, molecular weight 10 000, 99%, Shanghai Hansi Chemical Industry Co., Ltd.) were used to graft PEI onto the surface of Fe_3O_4@SiO_2. 1,4,5,8-Naphthalenetetracarboxylic-dianhydride (NTDA), *N*-methyl kelopyrrolidide (NMP) and methane sulfonic acid were purchased from Shanghai Macklin Biochemical Co., Ltd. and were used to functionalize Fe_3O_4@SiO_2@PEI. The reagents HCl, HNO_3, and NaOH were purchased from Tianjin Fengchuan. All solutions of Pb^{2+}, Cd^{2+}, Ni^{2+}, Cu^{2+} and Zn^{2+} (Merck Chemical Technology Co., Ltd., Shanghai, China) were prepared using doubly distilled water.

2.2. Apparatus

X-ray diffraction (XRD) patterns were acquired on a Bruker D8 Advance diffractometer using Cu Kα radiation in the angular range from 5° to 90° to analyze the crystal structures of the samples. Scanning electron microscopy (SEM) (JSM-6490LV) and field emission scanning electron microscopy (FESEM) (JEOL, JSM-7001F) were used to observe the surface structures of the samples. The core–shell structures and sizes of the samples were confirmed by high-resolution transmission electron microscopy (HRTEM) (JEOL, JEM-2100). Infrared absorption spectra were collected using a Fourier transform infrared (FT-IR) spectrometer (NICOLET 380) to analyze the compositions of the samples. A thermogravimetric analyzer (TGA, Diamond, Japan) was used to collect the weight loss curves of the samples at a heating rate of 10 °C min^{-1} to 1000 °C under an N_2 flow of 200 mL min^{-1}. Atomic absorption spectroscopy (AAS) (ContrAA-700) was used to determine the metal ion concentrations in the solutions. A high field vibrating sample magnetometer (LS7307-9309) was used to evaluate the magnetic properties of the samples.

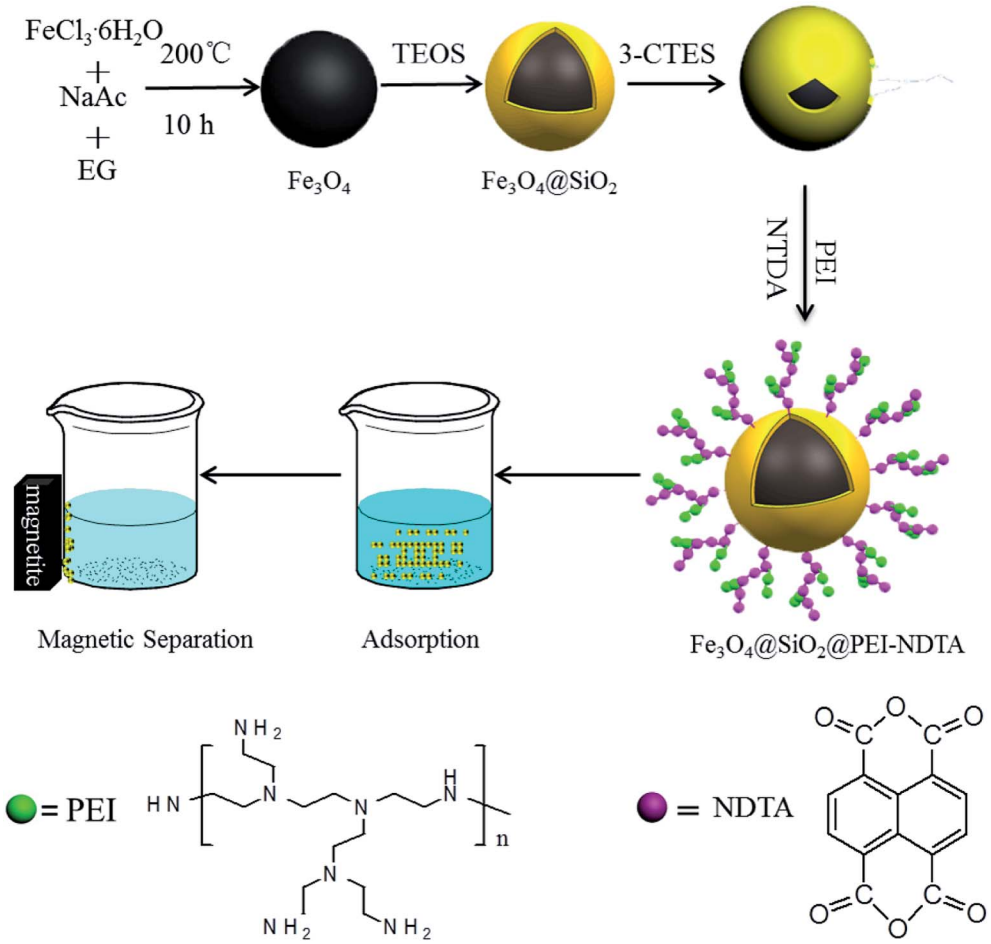

Scheme 1 The diagram of the synthesis process of Fe_3O_4@SiO_2@PEI-NTDA NPs and their application in Pb^{2+} removal.

2.3. Synthesis of Fe_3O_4 NPs

The magnetic Fe_3O_4 NPs were synthesized by the conventional solvothermal method.[31] In a typical procedure, 1.80 g $FeCl_3 \cdot 6H_2O$ and 1.09 g NaAc were added to 30 mL EG with vigorous stirring for 30 min; then, the mixture was heated at 200 °C in a sealed Teflon-lined stainless-steel autoclave with a volume of 50 mL for 12 h and naturally cooled to room temperature. The product was magnetically separated and washed with ethanol and deionized water, sequentially. The Fe_3O_4 NPs were dried under vacuum at 60 °C for 12 h.

2.4. Synthesis of Fe_3O_4@SiO_2 NPs

The Fe_3O_4@SiO_2 NPs were fabricated as reported previously.[32] Before coating Fe_3O_4 NPs with SiO_2, freshly prepared 100 mg Fe_3O_4 particles were dispersed in 100 mL HCl aqueous solution with a concentration of 0.1 mol L^{-1}; this mixture was placed in an ultrasonic bath for 15 min to form –OH groups on the outer surface of Fe_3O_4. Then, the hydroxylated Fe_3O_4 samples were washed thoroughly with deionized water to pH ~ 7.0 and re-dispersed in an ethanol/H_2O (80 mL/20 mL) mixture. $NH_3 \cdot H_2O$ (1.0 mL) was added to the above dispersion; then, 0.5 mL TEOS was introduced. The mixture was placed in an ultrasonic bath for 10 min, followed by mechanical stirring for 6 h at room temperature. Then, the synthesized Fe_3O_4@SiO_2 products were magnetically separated and washed with deionized water and ethanol several times, followed by vacuum drying at 60 °C for 12 h.

2.5. Synthesis of Fe_3O_4@SiO_2@PEI-NTDA

In a representative procedure, Fe_3O_4@SiO_2 NPs were treated with an aqueous solution of methane sulfonic acid (10%) as an activation reagent. The activated Fe_3O_4@SiO_2 NPs and 0.1 mL 3-chloropropyltrimethoxysilane were mixed in 30 mL xylene. The mixture was added to a Teflon-lined stainless-steel autoclave with a volume of 50 mL in an oven and maintained at 130 °C for 24 h. After that, the autoclave was cooled to room temperature and opened; then, PEI solution (10%) was added. The autoclave was then resealed, and the reaction was continued at 130 °C for another 24 h. The crude Fe_3O_4@SiO_2@PEI samples were separated and washed thoroughly with deionized water and ethanol. Vacuum drying was carried out at 60 °C for 12 h. Also, 50 mg of Fe_3O_4@SiO_2@PEI NPs was suspended in 150 mL *N*-methyl kelopyrrolidide under vigorous mechanical stirring, followed by adding 0.134 g NTDA. The mixture was further maintained at 60 °C under stirring for 6 h. The products denoted as

Fe_3O_4@SiO_2@PEI-NTDA NPs were obtained by magnetic separation, followed by washing and vacuum drying at 60 °C for 12 h.

2.6. Adsorption experiments

The adsorption properties of the Fe_3O_4@SiO_2@PEI-NTDA samples were estimated by batch experiments. In a typical process, a certain amount of Fe_3O_4@SiO_2@PEI-NTDA was added to a plastic tube containing 50 mL aqueous solution at room temperature with different initial concentrations of heavy metal ions (Pb^{2+}, Cd^{2+}, Ni^{2+}, Cu^{2+}, and Zn^{2+}), pH values, adsorption times, adsorbent dosages and coexisting pH values and adsorbent dosages. The tube was sealed and left for a certain contact time. After the adsorption experiments, the adsorbents were magnetically separated and the metal concentration in the residual solution was tested to determine the adsorption capacity of the adsorbent according to the following equation:

$$Q = \frac{(C_i - C_t)}{M} V \quad (1)$$

Here, Q stands for the adsorption capacity of the adsorbent (mg g^{-1}), C_i stands for the initial metal ion concentration in the solution (mg L^{-1}), C_t refers to the residual metal ion concentration (mg L^{-1}), M stands for the mass (g) of the adsorbent, and V stands for the volume of the solution (L).

In order to evaluate the selectivity of the prepared Fe_3O_4@SiO_2@PEI-NTDA adsorbent for Pb^{2+} over other metal ions, namely, Cd^{2+}, Ni^{2+}, Cu^{2+}, and Zn^{2+}, adsorption experiments were conducted with a contact time of 3 h by adding 25 mg Fe_3O_4@SiO_2@PEI-NTDA NPs to 50 mL solution (pH = 6.0) containing Pb^{2+}, Cd^{2+}, Ni^{2+}, Cu^{2+}, and Zn^{2+}, each of which had an initial concentration of 200 mg L^{-1}.

2.7. Leaching test

The material stability of Fe_3O_4@SiO_2@PEI-NTDA NPs was evaluated by the ratio of the mass of Fe_3O_4 leached by HCl solution to the total mass of the Fe_3O_4@SiO_2@PEI-NTDA adsorbent. The specific process is as follows: 10 mg of the Fe_3O_4@SiO_2@PEI-NTDA adsorbent was immersed in 50 mL of HCl solution for a certain interval; the Fe_3O_4@SiO_2@PEI-NTDA NPs were removed magnetically from the solution, and the residual solution was used to test the Fe ion concentration by AAS technology. The Fe ions in the solution, which were considered to have leached from Fe_3O_4@SiO_2@PEI-NTDA NPs by acid, were concerted into the mass of Fe_3O_4. The percentage was calculated by the mass of leached Fe_3O_4 to the total mass of Fe_3O_4@SiO_2@PEI-NTDA NPs to evaluate their stability under acidic conditions.

2.8. Desorption and recycling studies of Fe_3O_4@SiO_2@PEI-NTDA

Adsorption–desorption cycling experiments were carried out to investigate the reusability of the adsorbents. For one adsorption–desorption cycling procedure, 25 mg Fe_3O_4@SiO_2@PEI-NTDA sorbent was dispersed in 50 mL of aqueous solution with an initial Pb^{2+} concentration of 100 mg L^{-1} at an initial pH value of 6.0. After a contact time of 3 hours, the adsorbents were separated magnetically and the residual solution was subjected to Pb^{2+} measurements to calculate the adsorption capacity. The Pb^{2+}-loaded sorbent was followed by the desorption experiment, in which the Pb^{2+}-loaded sorbent was added to 30 mL of 0.5 M HCl solution under mechanical stirring at 350 rpm and at room temperature for 1 h. The Fe_3O_4@SiO_2@PEI-NTDA NPs were obtained by magnetic separation and washed to neutral pH with deionized water to prepare for the next adsorption–desorption cycling experiment. The adsorption–desorption cycling experiments were carried out for six times.

3. Results and discussion

3.1. The synthesis and structure of Fe_3O_4@SiO_2@PEI-NTDA NPs

Fe_3O_4 NPs, serving as the magnetic core of the adsorbent, were fabricated by a conventional solvothermal method. Fe_3O_4 NPs were coated with an SiO_2 layer by a conventional sol–gel method by hydrolyzing and condensing TEOS. Fe_3O_4@SiO_2 NPs were modified with a common silane coupling agent, 3-chloropropyltrimethoxysilane (CPTES), the Cl end groups of which can be used to react with the –NH– groups of a PEI polymer to form covalent grafting of branched PEI on the surface of Fe_3O_4@SiO_2. Afterward, the synthesized Fe_3O_4@SiO_2@PEI particles were further anhydride-functionalized with NTDA by the reaction between the –NH– groups and the anhydride groups of NTDA to construct Fe_3O_4@SiO_2@PEI-NTDA NPs.

The surface structures of the synthesized samples were observed by SEM. As shown in Fig. 1a, the prepared Fe_3O_4 samples are in good spherical shape and have a rough surface and a uniform particle size with diameter of about 200 nm. The diameter of Fe_3O_4 NPs can also be verified by the TEM images in Fig. 1d, where it ranges from 180 to 220 nm. As shown in Fig. 1b, Fe_3O_4@SiO_2 NPs have relatively smooth surfaces and large diameters compared to uncoated Fe_3O_4 NPs. Moreover, the TEM images in Fig. 1e show that the prepared Fe_3O_4@SiO_2 NPs have well-defined core–shell structures with homogeneous dense SiO_2 shells with thickness of approximately 20 nm. These results indicate that the SiO_2 layers were formed successfully on the surface of Fe_3O_4 spherical particles. This dense SiO_2 layer was expected to serve as a protective layer, protecting the magnetic Fe_3O_4 core from corrosion and oxidation in the adsorption process. The SEM images in Fig. 1c show that the Fe_3O_4@SiO_2@PEI-NTDA samples have homogeneous spherical particles, which are larger than those of Fe_3O_4@SiO_2, and this can also be verified by the TEM images. As shown in Fig. 1f, Fe_3O_4@SiO_2@PEI-NTDA NPs with diameters ranging from 200 to 300 nm have a core–shell structure with a dark core, which is assigned to Fe_3O_4. The light-transparent shell with irregular edges has thickness of about 30 nm, which is greater than that of the SiO_2 shell, indicating the successful grafting of PEI and successive modification with NTDA on Fe_3O_4@SiO_2. The successful grafting of PEI/NTDA was also confirmed by the EDXS measurements. As shown in Fig. 1g, the appearance of C, N and O signals can be attributed to the –NH– and –COOH

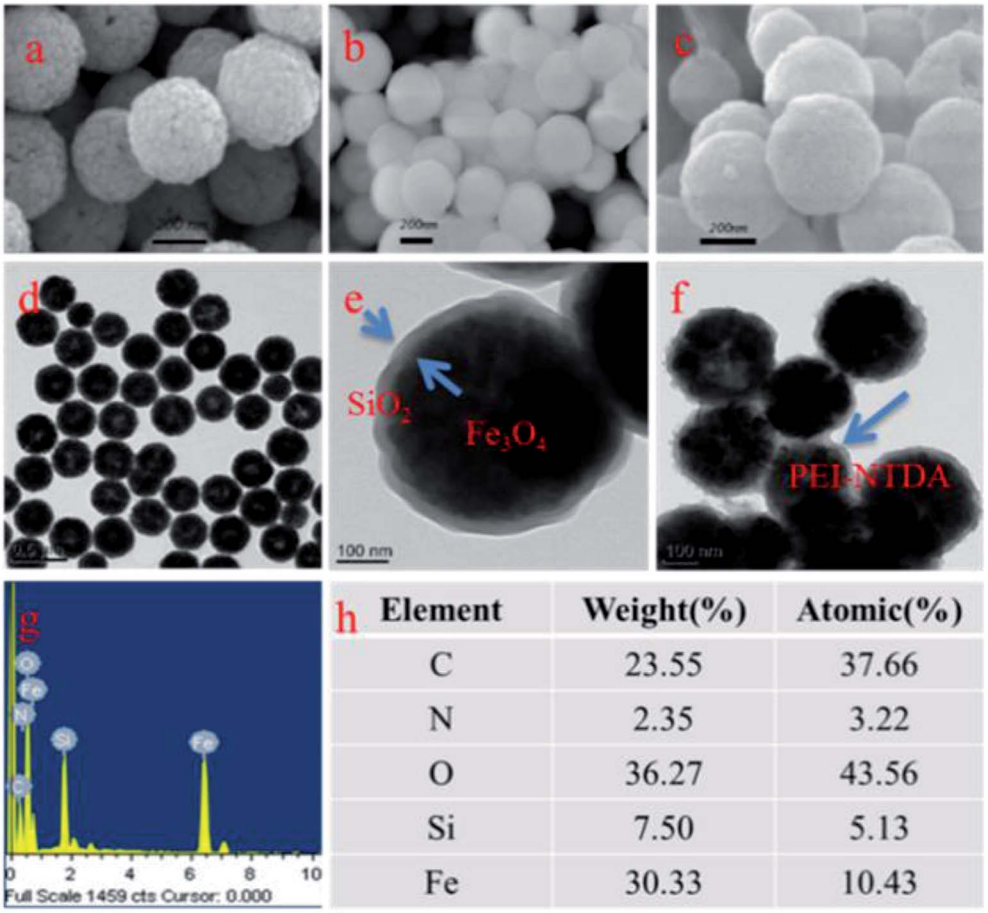

Fig. 1 SEM (a–c) and TEM (d–f) images of Fe_3O_4 NPs, Fe_3O_4@SiO_2, and Fe_3O_4@SiO_2@PEI-NTDA NPs, respectively; EDXS analysis (g and h) of Fe_3O_4@SiO_2@PEI-NTDA.

groups on PEI and NTDA. This outer PEI-NTDA layer is hydrophilic and contains numerous functional groups, which are expected to improve the adsorption capacity of the adsorbent by chelating with heavy metal ions for wastewater treatment.

Fe_3O_4 in the prepared composites has a face-centered cubic structure,[33,34] which is consistent with the JCPDS card (file no. 19-0629). Additionally, the positions of these characteristic peaks of Fe_3O_4 did not change in the XRD patterns of Fe_3O_4@SiO_2 and Fe_3O_4@SiO_2@PEI-NTDA, indicating that the binding process of the introduction of SiO_2 and the NTDA-functionalized PEI layer did not affect the crystal structure of Fe_3O_4. However, the characteristic diffraction peaks of Fe_3O_4 became relatively weak in the latter functionalized composites Fe_3O_4@SiO_2 and Fe_3O_4@SiO_2@PEI-NTDA, which may be due to the coating of amorphous SiO_2 and PEI.

The FT-IR spectra of all samples were obtained in the range from 4000^{-1} to 400 cm^{-1} to investigate the surface functional groups and confirm the chemical compositions of the modified NPs, as depicted in Fig. 2b. For pure Fe_3O_4 NPs, an obvious adsorption peak appears at 584 cm^{-1}, which is attributed to the characteristic Fe–O bond vibration from Fe_3O_4. After the sol–gel reaction with TEOS in the presence of Fe_3O_4, a new strong adsorption peak appeared at around 1100 cm^{-1}, which was attributed to the stretching vibrations of Si–O–Si and Si–O–H; this indicates the presence and successful coating of the SiO_2 layer on the samples of Fe_3O_4@SiO_2 and their successive samples of Fe_3O_4@SiO_2@PEI and Fe_3O_4@SiO_2@PEI-NTDA.[35] It can be observed in the FT-IR spectra of Fe_3O_4 and Fe_3O_4@SiO_2 NPs that two peaks for the stretching vibration of hydroxyl (–OH) groups appear at 1609 cm^{-1} and 3440 cm^{-1}, indicating that there are hydroxyl groups on the surfaces of Fe_3O_4 and Fe_3O_4@SiO_2 NPs. After the graft reaction with PEI, two new peaks at 2919 and 2840 cm^{-1} may be assigned to aliphatic C–H bonds; the bands at 1450 and 1320 cm^{-1} may belong to the stretching vibrations of C–H and C–N bonds, respectively.[28] The characteristic adsorption peaks of primary amines (–NH) appear at 1656 cm^{-1} and 1612 cm^{-1}, and a broader adsorption peak in the region of 3300–3600 cm^{-1} may be ascribed to the overlapping of the N–H vibration of PEI with the O–H stretching of SiO_2. All these results indicate the successful grafting of PEI. After reaction with NTDA, a new strong peak appears at 1680–1780 cm^{-1}, which may be attributed to the symmetric and asymmetric stretchings of –C=O bonds;[36] also, the peak at 1320 cm^{-1} (C–N asymmetric) indicates the successful functionalization of anhydride on the surface of Fe_3O_4@SiO_2.

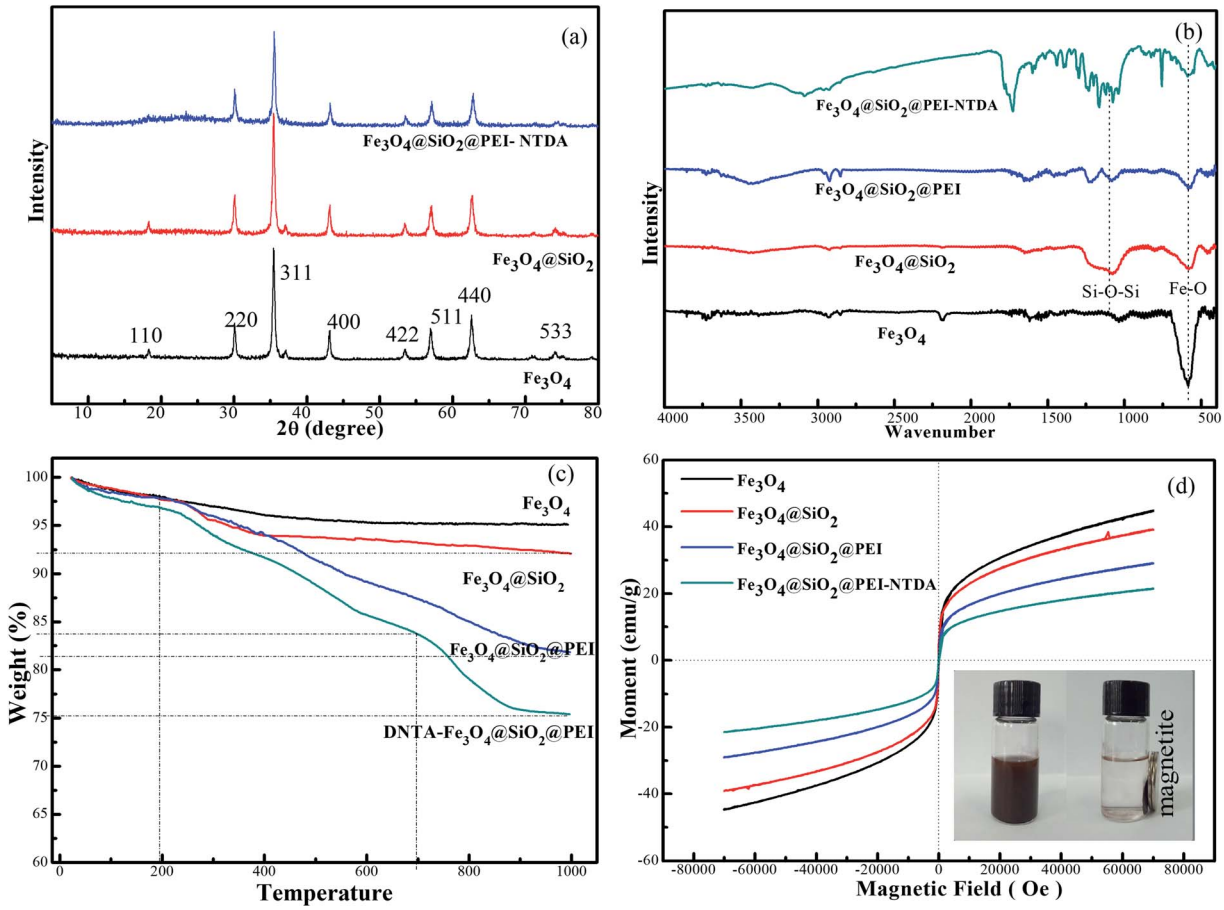

Fig. 2 XRD patterns (a), FT-IR spectra (b), TGA curves (c) and magnetization curves (d) of the samples.

TGA analyses of Fe_3O_4, Fe_3O_4@SiO_2, Fe_3O_4@SiO_2@PEI and Fe_3O_4@SiO_2@PEI-NTDA were also performed (Fig. 2c). It can be seen that Fe_3O_4 NPs displayed a weight loss of 4.83% in the range of 25–400 °C and remained stable above 400 °C. The obvious weight loss of Fe_3O_4@SiO_2 above 200 °C compared to that for pure Fe_3O_4 can be attributed to the structure decomposition of SiO_2. Also, the TGA curve of Fe_3O_4@SiO_2@PEI shows a dramatic decline above 400 °C, indicating the pyrolysis of PEI. The TGA curve of Fe_3O_4@SiO_2@PEI-NTDA displays one more step than that of Fe_3O_4@SiO_2@PEI above 700 °C, which can be attributed to NTDA. The weight losses of Fe_3O_4@SiO_2, Fe_3O_4@SiO_2@PEI and Fe_3O_4@SiO_2@PEI-NTDA at 1000 °C were 7.94%, 18.18% and 24.61%, respectively. These results also verified that PEI was grafted successfully on the surface of Fe_3O_4@SiO_2 and NTDA was successfully anchored on PEI.

The magnetization curves of the samples were all tested at room temperature (Fig. 2d). It can be observed that there are no hysteresis loops in the magnetization curves for all of the four samples. All of the samples are superparamagnetic. The magnetic saturation (M_s) value was found to be 44.7 emu g^{-1} for Fe_3O_4. Along with the modification processes on Fe_3O_4, the nonmagnetic layer sizes increased due to silica coating, PEI grafting and NTDA modification, due to which the M_s values decreased accordingly to 39.2 emu g^{-1} for Fe_3O_4@SiO_2, to 29.4 emu g^{-1} for Fe_3O_4@SiO_2@PEI, and to 21.6 emu g^{-1} for Fe_3O_4@SiO_2@PEI-NTDA.[37] Nevertheless, the value of Fe_3O_4@SiO_2@PEI-NTDA NPs was still high enough, due to which they could be completely separated from their aqueous dispersion by a magnet near the glass vial, affording a clear and transparent solution (inset photographs in Fig. 2d). These results indicate that Fe_3O_4@SiO_2@PEI-NTDA NPs are ready for use as magnetically separable adsorbents for application in water treatment.

3.2. Adsorption properties of Fe_3O_4@SiO_2@PEI-NTDA for Pb^{2+} heavy metal ion removal

In order to illustrate the advantages of Fe_3O_4@SiO_2@PEI-NTDA, batch experiments were carried out to test its adsorption properties for Pb^{2+} heavy metal ion removal at a temperature of 298 K, solution pH value of 6.0, sorbent dosage of 0.5 g L^{-1}, and contact time of 3 h. The results compared with those of Fe_3O_4@SiO_2 and Fe_3O_4@SiO_2@PEI are presented in Fig. 3. It can be observed that the adsorption capacity for Pb^{2+} removal is very low on Fe_3O_4@SiO_2 NPs, becomes higher on Fe_3O_4@SiO_2@PEI and reaches the highest value on Fe_3O_4@SiO_2@PEI-NTDA NPs; these results can be ascribed to the binding capability of the amino groups and functionalized carboxyl groups in the outer PEI-NTDA layer. This indicates that the modification methods employed in this work were effective to improve the adsorption properties of the magnetic sorbent Fe_3O_4.

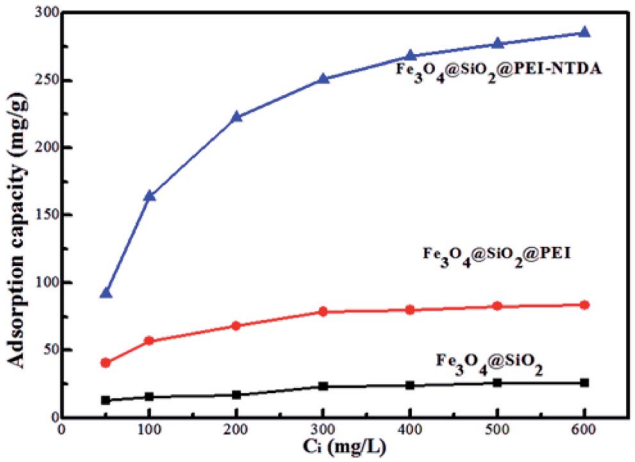

Fig. 3 Adsorption capabilities of Fe_3O_4@SiO_2, Fe_3O_4@SiO_2@PEI, and Fe_3O_4@SiO_2@PEI-NTDA for removal of Pb^{2+} from water. Adsorption conditions: sorbent dosage of 0.5 g L^{-1}, solution pH value of 6.0, equilibrium time of 3 h, temperature of 298 K.

Then, the influencing factors, including pH value, adsorbent dosage, initial Pb^{2+} concentration, contact time, and coexisting heavy ions, were optimized for the Pb^{2+} adsorption performance of Fe_3O_4@SiO_2@PEI-NTDA NPs. It has been reported that the adsorbent dosage has a significant effect on the interactions between the metal ions in the solution and the adsorption sites in the adsorbents[38] and further influences the adsorption capacity. Therefore, the Fe_3O_4@SiO_2@PEI-NTDA dosage was optimized by batch adsorption experiments by varying the adsorbent doses from 0.125 g L^{-1} to 1.0 g L^{-1}. The changes in the adsorption capacities with the adsorbent dosage are presented in Fig. 4a. The results showed that the adsorption capacity of Fe_3O_4@SiO_2@PEI-NTDA increased greatly with increasing dosage from 0.125 g L^{-1}; above the dosage of 0.5 g L^{-1}, continued increase in the dosage to 1.0 g L^{-1} resulted in a sharp decrease in the capacity. This can be explained as follows: when maintaining a constant initial Pb^{2+} concentration in the solution, the primary increase in the dosage may provide more available adsorption sites, leading to higher removal efficiency and higher adsorption capacity. When the dosage of the adsorbents matched the total quantity of Pb^{2+} in the solution, the adsorption capacity reached the highest value. Afterwards, further increase in the dosage may result in excessive adsorption sites and aggregation of the adsorbents, reducing the effective active adsorption sites for the removal of Pb^{2+} and hence the adsorption capacity.[21] It can be concluded from Fig. 4a that Fe_3O_4@SiO_2@PEI-NTDA NPs exhibit a higher adsorption capacity with a dosage of about 0.5 g L^{-1}, and the

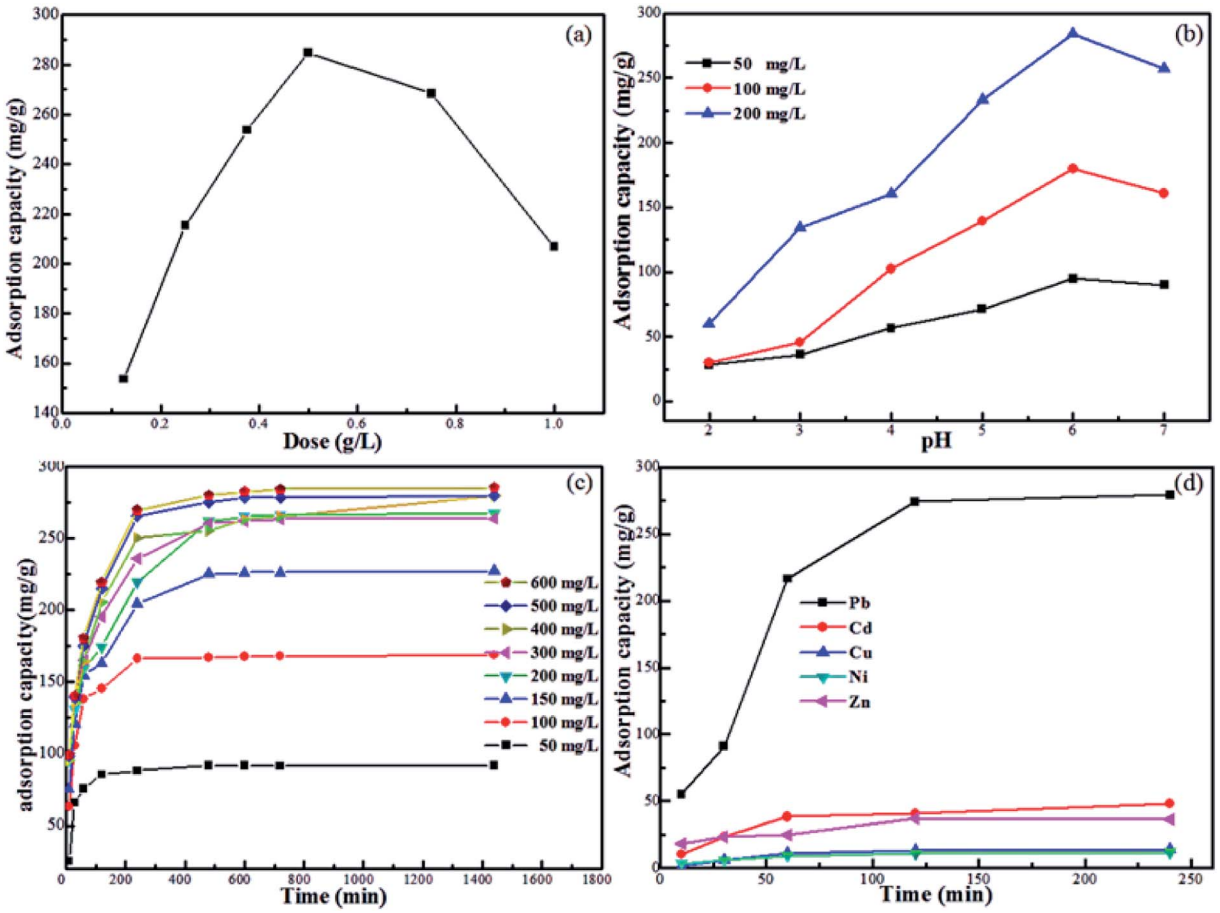

Fig. 4 Effects of (a) dosage, (b) pH, (c) contact time and initial Pb^{2+} concentration, and (d) coexisting heavy ions on Pb^{2+} adsorption of Fe_3O_4@SiO_2@PEI-NTDA NPs.

following adsorption experiments were conducted at this optimum dosage.

It is very important to select an appropriate pH for the adsorption process of Pb^{2+} removal because the pH value has significant influences on the surface charges of the sorbents in aqueous solutions, the ionization degree of the heavy metal ions and therefore the speciation of the adsorbate.[39] The optimized pH of Pb^{2+} adsorption was investigated (Fig. 4b). At low pH values below 6.0, it can be observed that the adsorption capacities of Fe_3O_4@SiO_2@PEI-NTDA increased obviously on increasing the solution pH and then decreased when the pH further increased from 6.0. At low pH values, the concentration of hydrogen (H^+) or hydronium (H_3O^+) ions increased with the decrease in the pH value, and competitive adsorption existed between the hydrogen (H^+) or hydronium (H_3O^+) ions and Pb^{2+} on the surface of the Fe_3O_4@SiO_2@PEI-NTDA adsorbents;[40] thus, the metal ions were inaccessible. On increasing pH, the competitive effect of H_3O^+ decreased, due to which the uptake of Pb^{2+} occurred more easily on the free binding sites. In addition, the speciation of lead is also dependent on the pH value. At pH values of 2.0–6.0, lead species exist exclusively as Pb^{2+} ions in the solution; above pH of 6.0, they will undergo hydrolysis to $Pb(OH)^+$ and the insoluble precipitate $Pb(OH)_2$.[41] The predominant adsorbing forms of lead are Pb^{2+} ions, which may interact with Fe_3O_4@SiO_2@PEI-NTDA *via* the carboxyl, hydroxyl and amino functional groups by a complexation mechanism. It can be observed that the maximum removal (285.3 mg g^{-1}) is achieved at about pH = 6.0. Therefore, further adsorption experiments were all carried out with an initial pH value of 6.0.

Adsorption equilibrium time experiments were conducted at a fixed adsorbent dosage of 0.5 g L^{-1} and an initial pH value of 6.0 for Pb^{2+} ion removal while varying the initial Pb^{2+} concentration from 50 to 600 mg L^{-1}. It can be observed from Fig. 4c that the adsorption of Pb^{2+} ions increases rapidly with contact time for the first 100 min at the beginning of the adsorption; this can be attributed to the abundant active adsorption sites that are available for easily interacting with Pb^{2+} ions. After that, the adsorption rate tended to become almost constant and finally, sorption equilibrium for the adsorption of Pb^{2+} ions was established in a dynamic balance between the concentration of Pb^{2+} ions in the solution and the adsorption sites on the adsorbent.

The adsorption rate and capacity of Fe_3O_4@SiO_2@PEI-NTDA increased on increasing the initial metal ion concentration of the solution. This can be explained by the fact that a higher initial Pb^{2+} ion concentration will provide a larger driving force between the solid–liquid interfaces to overcome the resistance during the mass transfer process, resulting in a higher adsorption rate. For all the initial Pb^{2+} ion concentrations employed in this work, an adsorption time of 200 min was sufficient to reach adsorption equilibrium. The competitive adsorption performance on Fe_3O_4@SiO_2@PEI-NTDA was investigated in the presence of coexisting Pb^{2+}, Cd^{2+}, Ni^{2+}, Cu^{2+}, and Zn^{2+} ions. As presented in Fig. 4d, Fe_3O_4@SiO_2@PEI-NTDA NPs exhibit much higher removal efficiency for Pb^{2+} than that for other metal ions, which is in the following order: Pb^{2+} > Cd^{2+} > Zn^{2+} > Cu^{2+} > Ni^{2+}. According to the Pearson hard–soft acid–base theory, Pb^{2+} can be classified as a borderline acid and prefers bonding to ligands containing N donor atoms. Fe_3O_4@SiO_2@PEI-NTDA with a large number of N atoms in the polymer resin may coordinate to Pb^{2+} rather than to Cd^{2+}, which is classified as a soft acid.

In order to determine the rate-controlling step of the adsorption process, including mass transport and chemical reactions, the data of the adsorption experiments were analyzed by the pseudo-first order[42] and the pseudo-second order[43] equations.

The pseudo-first order equation is expressed as follows:

$$\log(q_e - q_t) = \log q_e - \frac{K_1}{2.303} t \quad (2)$$

Here, q_t and q_e (mg g^{-1}) refer to the amounts of Pb^{2+} adsorbed on the adsorbent at time t and at equilibrium, respectively; K_1 (min^{-1}) refers to the rate constant. The plots of $\log(q_e - q_t)$ *versus* t are presented in Fig. 5a; from their slopes, the K_1 values are obtained and listed in Table 1.

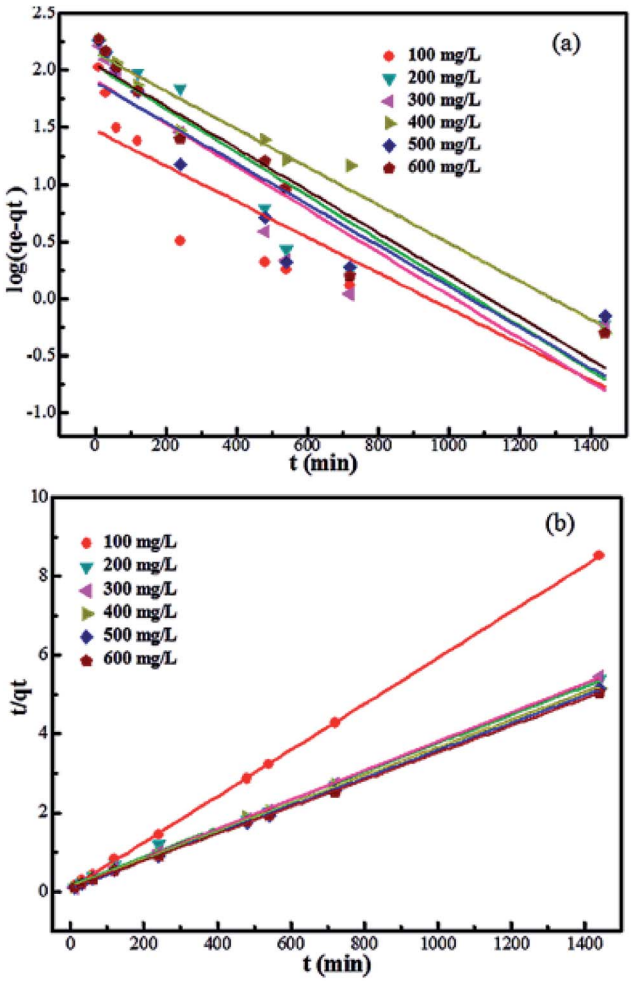

Fig. 5 Pseudo-first order model (a) and pseudo-second order model (b) for the adsorption of Pb^{2+} on Fe_3O_4@SiO_2@PEI-NTDA at dosage = 0.5 g L^{-1}, pH = 6.0, Pb^{2+} concentration = 200 mg L^{-1}, contact time = 3 h, and temperature = 298 K.

Table 1 Calculated pseudo-first-order and pseudo-second-order parameters for the adsorption of Pb^{2+}

Pb^{2+} conc. (mg L^{-1})	Pseudo-first-order			Pseudo-second-order		
	q_e (cal)	K_1 (min^{-1})	R^2	q_e (cal)	K_2 (g mg^{-1} min^{-1})	R^2
100	29.92	0.0035	0.710	171.2	0.00584	0.999
200	111.2	0.0043	0.839	277.7	0.00360	0.996
300	81.8	0.0043	0.798	271.0	0.00369	0.999
400	142.1	0.0038	0.964	284.9	0.00351	0.999
500	79.58	0.0041	0.788	286.5	0.00349	0.999
600	113.1	0.0042	0.909	292.3	0.00342	0.999

The pseudo-second order equation is given as follows:

$$\frac{t}{q_t} = \frac{1}{K_2 q_e^2} + \frac{1}{q_e} t \quad (3)$$

Here, K_2 (g (mg min)$^{-1}$) refers to the rate constant and q_t and q_e (mg g^{-1}) refer to the amounts of Pb^{2+} adsorbed on the adsorbent at time t and at equilibrium, respectively. Similarly, K_2 can be obtained from the plot of t/q_t *versus* t (Fig. 5b), and the results are listed in Table 1.

From Fig. 5, we can see that the pseudo-second order model fits the experiment data well; this can be confirmed by the correlation coefficient (R^2) values beyond 0.996, which are much higher than that of the pseudo-first order model (below 0.964). In addition, the values of the experimental adsorption capacity of the adsorbents are close to the calculated theoretical adsorption capacity ($q_{e,cal}$) from the pseudo-second order model. These results indicate that chemical adsorption may be the rate-limiting step of the adsorption process of Pb^{2+} on Fe_3O_4@SiO_2@PEI-NTDA.

For further understanding the adsorption mechanism of Pb^{2+} on Fe_3O_4@SiO_2@PEI-NTDA NPs, the Langmuir[44] and Freundlich[45] models were also applied to analyse the experimental adsorption data, which were obtained with an adsorbent dosage of m/V = 0.5 g L^{-1} and at pH = 6.0 at three different temperatures of 298 K, 303 K, and 308 K.

The Langmuir model is expressed by the following equation:

$$\frac{C_e}{q_e} = \frac{1}{q_m K} + \frac{C_e}{q_m} \quad (4)$$

Here, C_e (mg L^{-1}) refers to the metal ion concentration in the solution at equilibrium, q_e (mg g^{-1}) refers to the adsorption capacity on the sorbent at equilibrium, q_m (mg g^{-1}) refers to the monolayer adsorption capacity, and K refers to a Langmuir constant related to the sorption energy.

The Freundlich model is applicable to the adsorption that occurs on heterogeneous surfaces, and it is presented as follows:

$$\log q_e = \log K_f + \frac{1}{n} \log C_e \quad (5)$$

Here, K_f (mg g^{-1}) refers to a Freundlich constant related to the adsorption capacity and $1/n$ refers to an empirical parameter related to the adsorption intensity.

It can be observed from Fig. 6 that the adsorption isotherm data fit well with the Langmuir model than with the Freundlich model. The constant values and determination coefficients (R^2) are presented in Table 2. There is a high correlation regression equation R^2 value of 0.999 for the Langmuir model at each of the three experimental temperatures; it is far greater than that of the Freundlich model, which has a value of around 0.80. As we know, the Langmuir model is reasonable for a homogeneous adsorption process that takes place at the adsorbent surface, where there are no intermolecular interactions among the adsorbed molecules and all sites are identical and energetically

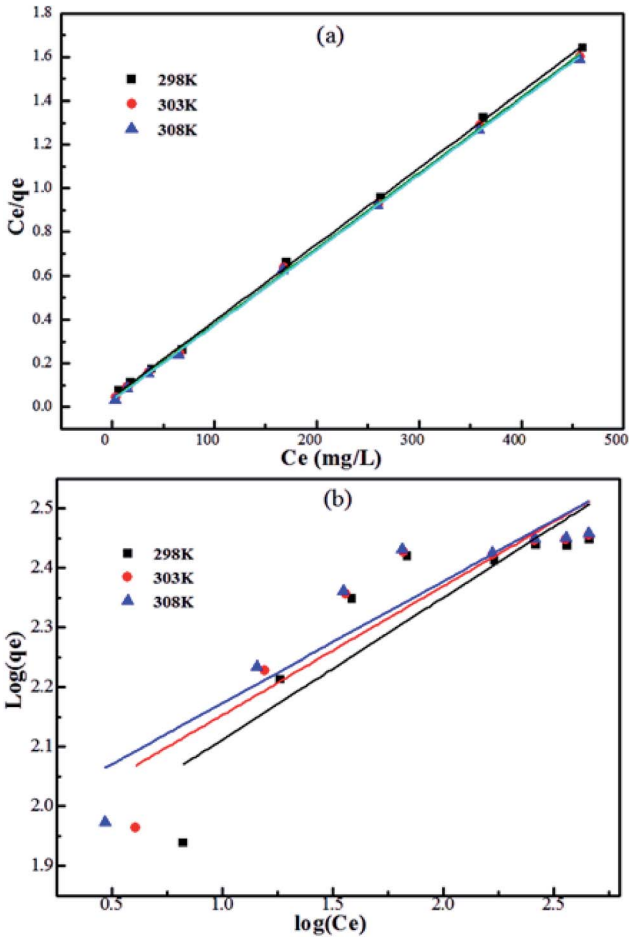

Fig. 6 Langmuir (a) and Freundlich (b) simulations for the adsorption of Pb^{2+} on Fe_3O_4@SiO_2@PEI-NTDA at dosage = 0.5 g L^{-1}, pH = 6.0, Pb^{2+} concentration = 200 mg L^{-1}, and contact time = 3 h at three different temperatures of 298 K, 303 K, and 308 K.

Table 2 Langmuir and Freundlich isotherm parameters for the adsorption of Pb^{2+} onto Fe_3O_4@SiO_2@PEI-NTDA at different temperatures

	Langmuir			Freundlich		
Temp. (K)	R^2	K	q_m	R^2	n	K_f
298	0.999	0.0786	286.9	0.756	4.20	74.77
303	0.999	0.0998	289.9	0.809	4.63	86.48
308	0.999	0.1128	290.7	0.836	4.89	92.99

equivalent for the adsorbate; the Freundlich model is applicable to adsorption that occurs on heterogeneous surfaces. These results reveal that the adsorption process of Pb^{2+} occurring on Fe_3O_4@SiO_2@PEI-NTDA may be uniform monolayer surface adsorption. The functional groups on the surface of Fe_3O_4@SiO_2@PEI-NTDA provide binding sites for Pb^{2+} to reach a high adsorption capacity. As shown in Table 3, the prepared Fe_3O_4@SiO_2@PEI-NTDA NPs possess remarkable adsorption capacity for Pb^{2+} compared to previously reported magnetic adsorbents.

3.3. Stability and cycling properties of Fe_3O_4@SiO_2@PEI-NTDA for heavy metal ions of Pb^{2+}

The material stability and regeneration of Fe_3O_4@SiO_2@PEI-NTDA were also studied to evaluate the repeated availability of the adsorbent in water treatment for economic consideration. It can be seen from the above adsorption results that the adsorption of Pb^{2+} on Fe_3O_4@SiO_2@PEI-NTDA is pH-dependent and that the optimum adsorption capacity occurs at a pH value of about 6.0. Additionally, in order to recover the adsorbent from the state of adsorption, a desorption process must be carried out by the treatment of the adsorbent with HCl solution. In these two cases, naked Fe_3O_4 may be subject to leaching from the adsorbents because of the acid media. Therefore, the material stability in acidic media is very important for the modified Fe_3O_4 adsorbent to evaluate its regeneration

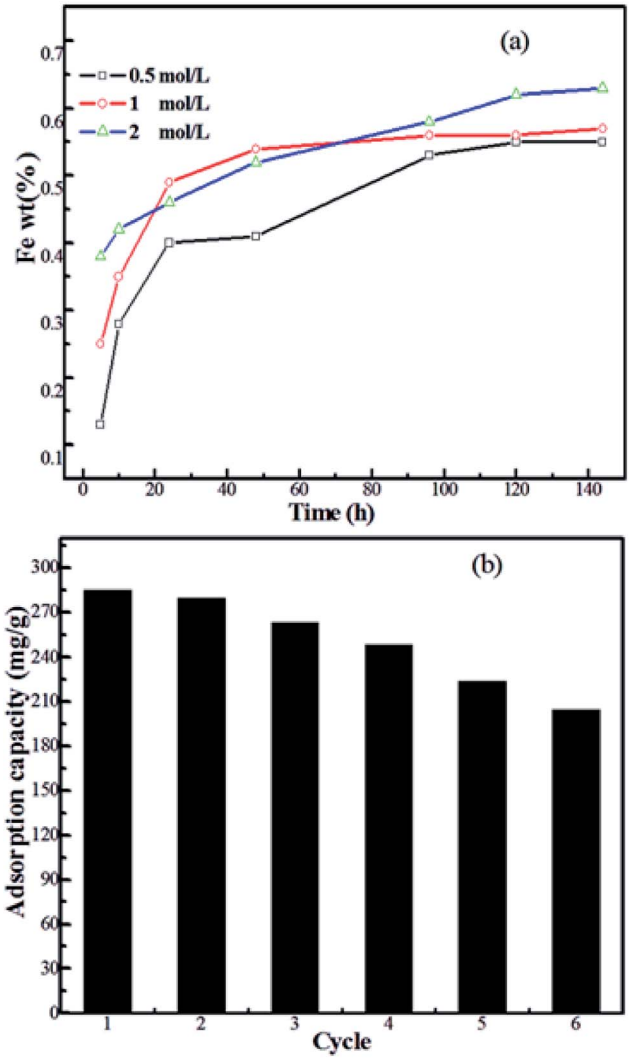

Fig. 7 (a) The leaching percentages of Fe from Fe_3O_4@SiO_2@PEI-NTDA in different HCl solutions; T = 298 K, dose = 0.5 g L^{-1}. (b) Recycling of Fe_3O_4@SiO_2@PEI-NTDA in the removal of Pb^{2+}; T = 298 K, dose = 0.5 g L^{-1}, pH = 6.0.

Table 3 Maximum capacities of Pb^{2+} on various magnetic adsorbents

	Adsorption capacities (mg g^{-1})		
Type of adsorbent	Pb^{2+}	Cd^{2+}	Ref.
Polymer-modified Fe_3O_4	83.3		46
PAA@TSH-modified Fe_3O_4	188.7	107.5	47
Amino-functionalized Fe_3O_4@SiO_2	76.6	22.5	48
PEI-functionalized mesoporous magnetic clusters	216.3		49
PEI-bacterial cellulose bio-adsorbent	141		50
Magnetic porous Fe_3O_4–MnO_2	208.2	169.9	51
Biochar–$MnFe_2O_4$	154.94	127.83	52
T-β-CD-Fe_3O_4	105.38		53
NTA-silica gel	76.22	53.14	54
Fe_3O_4@SiO_2@PEI-NTDA	**285.3**	**48.2**	**This work**

properties; this is carried out by soaking certain amounts of Fe_3O_4@SiO_2@PEI-NTDA in HCl solution with various concentrations for certain times. The Fe ion concentration in the solution was tested and the Fe leaching percent was calculated, as shown in Fig. 7a. It can be seen that the Fe leaching percent increases on increasing the soaking time and on increasing the concentration of HCl in the solution and reaches a lower value of 0.65 wt% after 144 h treatment in 2 mol L^{-1} HCl solution, indicating high material stability of the prepared Fe_3O_4@SiO_2@PEI-NTDA adsorbent in acid media. This can be attributed to the outer SiO_2@PEI layer, which functions as an effective protecting shell that enables Fe_3O_4@SiO_2@PEI-NTDA to be readily reused. Hence, adsorption–desorption experiments were carried out, and the adsorption capacity results of the recycling experiment are shown in Fig. 6b. It can be observed that the adsorption capacity decreased on increasing the recycling time and Fe_3O_4@SiO_2@PEI-NTDA remained valid

for Pb^{2+} removal for six times with a high adsorption capacity of 204.3 mg g^{-1}; this indicates that Fe_3O_4@SiO_2@PEI-NTDA is a promising adsorbent that can be applied repeatedly in water treatment for the removal of Pb^{2+}.

4. Conclusion

A novel magnetically separable adsorbent was successfully constructed with a core–shell structure comprising a magnetic Fe_3O_4 core, an outer protective SiO_2 layer and an outermost hydrophilic layer of PEI-NTDA with abundant functionalized groups including amino groups, hydroxyl and carboxyl groups, which could bind with heavy metal ions. This core–shell structure endowed Fe_3O_4@SiO_2@PEI-NTDA with many good properties: the composites are magnetically separable and sustainable in acid media with a low weight loss; also, Fe_3O_4@SiO_2@PEI-NTDA NPs have a high primary adsorption capacity of Pb^{2+} and the adsorbents can be recovered by HCl treatment for recycling, maintaining high recycling adsorption capacity of 204.3 mg g^{-1} for six adsorption–regeneration cycles. These unique properties make Fe_3O_4@SiO_2@PEI-NTDA NPs promising effective adsorbents for the removal of Pb^{2+} metal ions in water treatment.

Conflicts of interest

There are no conflicts to declare.

Acknowledgements

This work was supported by grants from the National Natural Science Foundation of China (No. 21401170, 21271160, 91022011, 21371092), National Basic Research Program of China (2010CB923303), Major Projects in Henan Province of China (No. 181100310300) and Research Fund for the Doctoral Program of Zhengzhou University of Light Industry (No. 2013BSJJ021).

References

1 F. Fu and Q. Wang, Removal of heavy metal ions from wastewaters: a review, *J. Environ. Manage.*, 2011, **92**(3), 407–418.
2 F. E. Peer, N. Bahramifar and H. Younesi, Removal of Cd (II), Pb (II) and Cu (II) ions from aqueous solution by polyamidoamine dendrimer grafted magnetic graphene oxide nanosheets, *J. Taiwan Inst. Chem. Eng.*, 2018, **87**, 225–240.
3 R. P. Medina, E. T. Nadres, F. C. Ballesteros and D. F. Rodrigues, Incorporation of graphene oxide into a chitosan-poly(acrylic acid) porous polymer nanocomposite for enhanced lead adsorption, *Environ. Sci.: Nano*, 2016, **3**, 638–646.
4 K. Li and X. Wang, Adsorptive removal of Pb(II) by activated carbon prepared from Spartina alterniflora: equilibrium, kinetics and thermodynamics, *Bioresour. Technol.*, 2009, **99**(11), 2810–2815.
5 D. Marani, G. Macchi and M. Pagano, Lead precipitaiton in the presence of sulphate and carbonate, testing the thermodynamic predictions, *Water Res.*, 1995, **29**(4), 1085–1092.
6 L. C. Lin and R. S. Juang, Ion-exchange equilibria of Cu(II) and Zn(II) from aqueous solutions with Chelex 100 and Amberlite IRC 748 resins, *Chem. Eng. J.*, 2005, **112**(1), 211–218.
7 J. S. George, A. Ramos and H. J. Shipley, Tanning facility wastewater treatment: Analysis of physical–chemical and reverse osmosis methods, *J. Environ. Chem. Eng.*, 2015, **3**(2), 969–976.
8 D. Sribudda, T. Wannachod and P. Ramakul, Separation of mercury and arsenic from produced water via hollow fiber contactor: Kinetic and mass transfer analysis, *Korean J. Chem. Eng.*, 2016, **33**(1), 1–10.
9 K. Dutta, S. Mukhopadhyay, S. Bhattacharjee and B. Chaudhuri, Chemical oxidation of methylene blue using a Fenton-like reaction, *J. Hazard. Mater.*, 2001, **84**(1), 57–71.
10 L. Luo, Y. Xie, Q. Liu, Z. Tan and X. Li, Isolation of a biological iron sulfide composites-producing strain and its application in emergency treatment of heavy metal wastewater, *Chin. J. Appl. Environ. Biol.*, 2012, **18**(01), 115–121.
11 V. K. Gupta, I. Ali, T. A. Saleh, A. Nayak and S. Agarwal, Chemical treatment technologies for waste-water recycling—an overview, *RSC Adv.*, 2012, **2**, 6380–6388.
12 J. S. Pang, A. H. Deng, L. B. Mao, J. Chen, X. J. Peng and J. Zhu, Adsorption of heavy metal ions with magnetic carbon-coated iron nanoparitcles, *Adv. Mater. Res.*, 2012, **490–495**, 3049–3053.
13 G. B. Baur, I. Yuranov and L. Kiwi-Minsker, Activated carbon fibers modified by metal oxide as effective structured adsorbents for acetaldehyde, *Catal. Today*, 2015, **249**, 252–258.
14 Q. Meng, H. Chen, Z. Lin and J. Sun, Zeolite A synthesized from alkaline assisted pre-activated halloysite for efficient heavy metal removal in polluted river water and industrial wastewater, *J. Environ. Sci.*, 2017, **56**, 254–262.
15 M. N. Sepehr, M. Zarrabi, A. Amrane and M. R. Samarghandi, Removal of Cr (III) from model solutions and a real effluent by Phanerochaete chrysosporium isolated living microorganism: equilibrium and kinetics, *Desalin. Water Treat.*, 2013, **51**(28–30), 5627–5637.
16 S. Dib, M. Boufatit, S. Chelouaou, F. Sadi-Hassaine, J. Croissant, J. Long, L. Raehm, C. Charnay and J.-O. Durand, Versatile heavy metals removal via magnetic mesoporous nanocontainers, *RSC Adv.*, 2014, **4**, 24838–24841.
17 T. S. Munonde, N. W. Maxakato and P. N. Nomngongo, Preparation of magnetic Fe_3O_4 nanocomposites modified with MnO_2, Al_2O_3, Au and their application for preconcentration of arsenic in river water samples, *J. Environ. Chem. Eng.*, 2018, **6**(2), 1673–1681.
18 C. Liu, X. Zhu, P. Wang, Y. Zhao and Y. Ma, Defects and interface states related photocatalytic properties in

reduced and subsequently nitridized Fe_3O_4/TiO_2, *J. Mater. Sci. Technol.*, 2018, **34**(6), 931–941.

19 Q. Wu, M. Li, Z. Huang, Y. Shao, L. Bai and L. Zhou, Well-defined nanostructured core–shell magnetic surface imprinted polymers (Fe_3O_4@SiO_2@MIPs) for effective extraction of trace tetrabromobisphenol A from water, *J. Ind. Eng. Chem.*, 2018, **60**, 268–278.

20 Q. Yang, S. S. Ren, Q. Zhao, R. Lu, H. Cheng, Z. Chen and H. Zheng, Selective separation of methyl orange from water using magnetic ZIF-67 composites, *Chem. Eng. J.*, 2017, **333**, 49–57.

21 Y. Ren, H. A. Abbood, F. He, H. Peng and K. Huang, Magnetic EDTA-modified chitosan/SiO_2/Fe_3O_4 adsorbent: Preparation, characterization, and application in heavy metal adsorption, *Chem. Eng. J.*, 2013, **226**(12), 300–311.

22 S. Zhang, Y. Zhang, J. Liu, Q. Xu, H. Xiao, X. Wang, H. Xu and J. Zhou, Thiol modified Fe_3O_4@SiO_2 as a robust, high effective, and recycling magnetic sorbent for mercury removal, *Chem. Eng. J.*, 2013, **226**(24), 30–38.

23 J. H. Wang, S. R. Zheng, Y. Shao, J. Liu, Z. Xu and D. Zhu, Amino-functionalized Fe_3O_4@SiO_2 core-shell magnetic nanomaterial as a novel adsorbent for aqueous heavy metals removal, *J. Colloid Interface Sci.*, 2010, **349**(1), 293–299.

24 Y. Yan, G. Yuvaraja, C. Liu, L. Kong, K. Guo, G. M. Reddy and G. V. Zyryanov, Removal of Pb(II) ions from aqueous media using epichlorohydrin crosslinked chitosan schiff's base@Fe_3O_4 (ECCSB@Fe_3O_4), *Int. J. Biol. Macromol.*, 2018, **117**, 1305–1313.

25 L. Yan, S. Li, H. Yu, R. Shan, B. Du and T. Liu, Facile solvothermal synthesis of Fe_3O_4/bentonite for efficient removal of heavy metals from aqueous solution, *Powder Technol.*, 2016, **301**, 632–640.

26 J. Li, Z. Shao, C. Chen and X. Wang, Hierarchical GOs/Fe_3O_4/PANI magnetic composites as adsorbent for ionic dye pollution treatment, *RSC Adv.*, 2014, **4**(72), 38192–38198.

27 Q. Zhang, M. He, B. Chen and B. Hu, Magnetic mesoporous carbons derived from in situ MgO template formation for fast removal of heavy metal ions, *ACS Omega*, 2018, **3**(4), 3752–3759.

28 S. Zhang, Z. Wang, H. Chen, C. Kai, M. Jiang, Q. Wang and Z. Zhou, Polyethylenimine functionalized Fe_3O_4/steam-exploded rice straw composite as an efficient adsorbent for Cr(VI) removal, *Appl. Surf. Sci.*, 2018, **440**, 1277–1285.

29 G. Bayramoglu and M. Y. Arica, Adsorption of Cr(VI) onto PEI immobilized acrylate-based magnetic beads: Isotherms, kinetics and thermodynamics study, *Chem. Eng. J.*, 2008, **139**(1), 20–28.

30 C. Xiao, X. Liu, S. Mao, L. Zhang and J. Lu, Sub-micron-sized polyethylenimine-modified polystyrene/Fe_3O_4/chitosan magnetic composites for the efficient and recyclable adsorption of Cu(II) ions, *Appl. Surf. Sci.*, 2017, **394**, 378–385.

31 T. Zhang, X. Zhang, X. Yan, L. Kong, G. Zhang, H. Liu, J. Qiu and K. L. Yeung, Synthesis of Fe_3O_4@ZIF-8 magnetic core–shell microspheres and their potential application in a capillary microreactor, *Chem. Eng. J.*, 2013, **228**(28), 398–404.

32 C. Hui, C. Shen, J. Tian, L. Bao, H. Ding, C. Li, Y. Tian, X. Shi and H. Gao, Core-shell Fe_3O_4@SiO_2 nanoparticles synthesized with well-dispersed hydrophilic Fe_3O_4 seeds, *Nanoscale*, 2011, **3**(2), 701–705.

33 L. Wang, D. Hu, X. Kong, X. Li, K. Zhou, H. Zhao and C. Zhou, Anionic polypeptide poly(γ-glutamic acid)-functionalized magnetic Fe_3O_4-GO-(o-MWCNTs) hybrid nanocomposite for high-efficiency removal of Cd(II), Cu(II) and Ni(II) Heavy metal ions, *Chem. Eng. J.*, 2018, **346**, 38–49.

34 Y. Zhang, W. Liu, Z. Li, M. Wang and M. Zhao, Application of bifunctional saccharomyces cerevisiae to remove lead(II) and cadmium(II) in aqueous solution, *Appl. Surf. Sci.*, 2011, **257**(23), 9809–9816.

35 N. Mir, A. Heidari, H. Beyzaei, S. Mirkazehi-Rigi and P. Karimi, Detection of Hg^{2+} in aqueous solution by pyrazole derivative-functionalized Fe_3O_4@SiO_2 fluorescent probe, *Chem. Eng. J.*, 2017, **327**, 648–655.

36 L. Cao, Q. Q. Sun, Y. H. Gao, L. T. Liu and H. F. Shi, Novel acid-base hybrid membrane based on amine-functionalized reduced graphene oxide and sulfonated polyimide for vanadium redox flow battery, *Electrochim. Acta*, 2015, **18**, 24–34.

37 J. Kim, H. S. Kim, N. Lee, T. Kim, H. Kim, T. Yu, I. C. Song, W. K. Moon and T. yeon, Multifunctional uniform nanoparticles composed of a magnetite nanocrystal core and a mesoporous silica shell for magnetic resonance and fluorescence imaging and for drug delivery, *Angew. Chem.*, 2008, **47**(44), 8438–8441.

38 W. S. W. Ngah, C. S. Endud and R. Mayanar, Removal of copper(II) ions from aqueous solution onto chitosan and cross-linked chitosan beads, *React. Funct. Polym.*, 2002, **50**(2), 181–190.

39 R. Katal, E. Hasani, M. Farnam, M. S. Baei and M. A. Ghayyem, Charcoal ash as an adsorbent for Ni(II) adsorption and Its application for wastewater treatment, *J. Chem. Eng. Data*, 2012, **57**(2), 374–383.

40 W. C. Kao, J. Y. Wu, C. C. Chang and J. Chang, Cadmium biosorption by polyvinyl alcohol immobilized recombinant escherichia coli, *J. Hazard. Mater.*, 2009, **169**(1–3), 651–658.

41 Z. F. Liu, G. M. Zeng, H. Zhong, X. Yuan, L. Jiang, H. Fu, X. Ma and J. Zhang, Effect of saponins on cell surface properties of penicillium simplicissimum: performance on adsorption of cadmium(II), *Colloids Surf., B*, 2011, **86**(2), 364–369.

42 C. Tamerler, E. E. Oren, M. Duman, E. Venkatasubramanian and M. Sarikaya, Adsorption kinetics of an engineered gold binding peptide by surface plasmon resonance spectroscopy and a quartz crystal microbalance, *Langmuir*, 2006, **22**(18), 7712–7718.

43 J. Ethève and D. Philippe, Adsorption kinetics of lysozyme on silica at pH 7.4: correlation between streaming potential and adsorbed amount, *Langmuir*, 2002, **18**(5), 1777–1785.

44 L. G. Yan, K. Yang, R. R. Shan, T. Yan, J. Wei, S. Yu, H. Yu and B. Du, Kinetic, isotherm and thermodynamic investigations of phosphate adsorption onto core-shell Fe_3O_4@LDHs composites with easy magnetic separation assistance, *J. Colloid Interface Sci.*, 2015, **448**, 508–516.

45 L. A. Rodrigues and M. L. C. P. D. Silva, Thermodynamic and kinetic investigations of phosphate adsorption onto hydrous niobium oxide prepared by homogeneous solution method, *Desalination*, 2010, **263**(1), 29–35.

46 S. Venkateswarlu and M. Yoon, Core-shell ferromagnetic nanorod based on amine polymer composite (Fe_3O_4@DAPF) for fast removal of Pb(II) from aqueous solutions, *ACS Appl. Mater. Interfaces*, 2015, **7**(45), 25362–25372.

47 K. Zargoosh, H. Abedini, A. Abdolmaleki and M. R. Molavian, Effective removal of heavy metal ions from industrial wastes using thiosalicylhydrazide-modified magnetic nanoparticles, *Ind. Eng. Chem. Res.*, 2013, **52**(42), 14944–14954.

48 J. Wang, S. Zheng, Y. Shao, J. Liu, Z. Xu and D. Zhu, Amino-functionalized Fe_3O_4@SiO_2 core-shell magnetic nanomaterial as a novel adsorbent for aqueous heavy metals removal, *J. Colloid Interface Sci.*, 2010, **349**(1), 293–299.

49 M. Y. Lee, J. H. Lee, J. W. Chung and S. Kwak, Hydrophilic and positively charged polyethylenimine-functionalized mesoporous magnetic clusters for highly efficient removal of Pb(II) and Cr(VI) from wastewater, *J. Environ. Manage.*, 2017, **206**, 740–748.

50 X. Jin, Z. Xiang, Q. Liu, Y. Chen and F. Lu, Polyethyleneimine-bacterial cellulose bioadsorbent for effective removal of copper and lead ions from aqueous solution, *Bioresour. Technol.*, 2017, **244**(1), 844–849.

51 J. Zhao, J. Liu, N. Li, W. Wang, J. Nan, Z. Zhao and F. Cui, Highly efficient removal of bivalent heavy metals from aqueous systems by magnetic porous Fe_3O_4-MnO_2: Adsorption behavior and process study, *Chem. Eng. J.*, 2016, **304**, 737–746.

52 L. Zhang, J. Guo, X. Huang, W. Wang, P. Sun, Y. Li and J. Han, Functionalized biochar-supported magnetic MnFe2O4 nanocomposite for the removal of Pb(II) and Cd(II), *RSC Adv.*, 2019, **9**, 365–376.

53 A. Abdolmaleki, S. Mallakpour and S. Borandeh, Efficient heavy metal ion removal by triazinyl-β-cyclodextrin functionalized iron nanoparticles, *RSC Adv.*, 2015, **5**, 90602–90608.

54 Y. Li, J. He, K. Zhang, T. Liu, Y. Hu, X. Chen, C. Wang, X. Huang, L. Kong and J. Liu, Super rapid removal of copper, cadmium and lead ions from water by NTA-silica gel, *RSC Adv.*, 2019, **9**, 397–407.